JOURNAL OF MATERIALS SCIENCE 25 (1990) 2727–2736

Electron microscopy of non-periodic layer crystallites in thermotropic random copolymers

RICHARD J. SPONTAK, ALAN H. WINDLE*
Department of Materials Science and Metallurgy, University of Cambridge, Pembroke Street, Cambridge CB2 3QZ, UK

Transmission electron microscopy (TEM) has been used to characterize non-periodic layer crystallites in thermotropic random copolyesters composed of 4-hydroxybenzoic acid and 2-hydroxy-6-naphthoic acid. The crystallites are most clearly observed when imaged in the equatorial reflection, indicating that they are associated with intermolecular ordering. The crystallites appear to be platelets with their thin axis parallel to the molecular chain axis. Crystallite growth is highly dependent on thermal history and occurs to a significant extent during the early stages of annealing above the glass-transition temperature in the solid state. Long-term annealing of the copolymers results in an increase in the number of crystallites, as well as sharpening the diffraction pattern. The extent of lateral development of the ordered regions also depends on the degree of polymerization (DP), being greater for a copolymer of lower DP.

1. Introduction

Some aromatic homopolyesters, such as those derived from 4-hydroxybenzoic acid (HBA) or 2-hydroxy-6-naphthoic acid (HNA) residues, retain their stable crystalline structure up to the temperature where they decompose, thereby making them intractable from a thermal processing standpoint. The problem is alleviated by building copolymers from the parent monomers, which have lower melting points and, of course, reduced crystallinity. The random copolymer molecules are sufficiently rigid and straight to exhibit liquid-crystalline characteristics between their melting point ($\approx 300°C$) and decomposition temperature above 400°C.

Several investigators [1–5] have reported aperiodic meridional X-ray diffraction maxima which are shown to be indicative of a true random copolymer, but the presence of a well-defined equatorial reflection (and sometimes off-equatorial ones) suggests a finite degree of crystalline order [6, 7]. In fact, Butzbach *et al.* [8], using X-ray analysis, have estimated that the degree of crystallinity in an HBA–HNA (58:42) copolymer could exceed 60% after very long anneal times, whereas Blundell [6] has measured 21% crystallinity in a similar (40:60) copolymer. The concentration of the first of the aperiodic intrachain maxima on the meridian, especially after annealing, has been interpreted in terms of a model in which similar but non-periodic sequences on neighbouring chains are in register [9]. Ordered regions formed in this way are referred to as non-periodic layer (NPL) crystallites and are shown schematically in Fig. 1.

After the conception of that initial scheme, Hanna and Windle [10] investigated and made predictions for the geometrical limitations on ordering in liquid-crystalline copolymers varying in both composition and molecular weight, and Golombok *et al.* [11] have demonstrated for a point model that NPL crystallites are consistent with the observed intensification of the meridian at the first intrachain layer line. The first direct observation of these crystallites was reported by Donald and Windle [12]. Using an annealed HBA–HNA (70:30) copolymer, the crystallites were imaged in dark-field TEM and appeared as platelets about 100 nm long and 20 nm thick in the chain direction. Further visual evidence of NPL crystallites has since been reported [5] in an etched sample of HBA–HNA (75:25) copolymer of lower molecular weight.

The objectives of this work are to use TEM imaging and image-analysis techniques to further an understanding of NPL crystallites in thermotropic random copolymers and to characterize the morphology of these crystallites in terms of processing conditions and molecular weight.

2. Experimental methods

The copolymers used here have been provided by the Hoechst-Celanese Corporation (Summit, New Jersey, USA) and are composed of 75 mol % HBA and 25 mol % HNA, as given below:

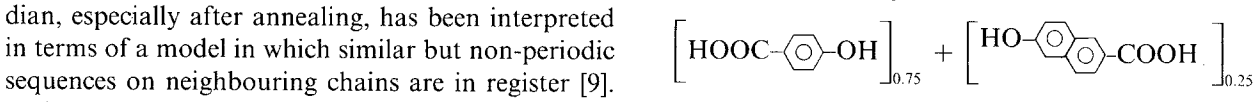

For convenience, this classification of copolymer will be hereafter denoted B–N. The high-molecular-weight (HMW) sample has a degree of polymerization (DP) of about 150, and the low-molecular-weight (LMW) one has a DP of approximately 25.

*To whom all correspondence should be addressed.

0022–2461/90 $03.00 + .12

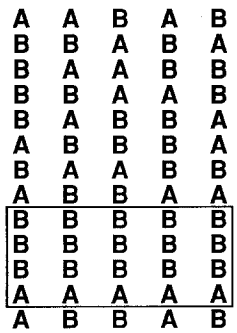

Figure 1 Schematic representation of a non-periodic layer (NPL) crystallite in a thermotropic random copolyester. These crystallites are the result of longitudinal register of adjacent identical sequences of monomer units.

To obtain specimens that are electron-transparent in conventional TEM, a variation of the method for producing ultrathin sheared films used by Donald and co-workers [12–17] was employed (see Fig. 2). Small sections of copolymer were cut from the pellets received and were placed on freshly-cleaved NaCl. The temperature of the specimen and substrate was increased to a designated temperature (T_s) at which shearing commenced. Once the sample had reached the temperature, it was quickly sheared with a freshly-sharpened razor blade and immediately quenched to 0° C on an aluminium block to "freeze in" the molecular orientation [18]. Unlike the previously used method of Donald and co-workers [12–17], the resulting films were then scored into sections that would fit on to the TEM copper grids, and the rocksalt substrate was dissolved prior to subsequent annealing in order to avoid substrate effects, such as surface-driven homeotropy [15]. After the ultrathin films, typically measuring about 100 nm thick, had been picked up on 100 × 200 mesh folding grids, they were annealed in an inert nitrogen atmosphere at a temperature (T_a) above the glass transition temperature ($T_g \approx 190°$ C) in the solid state for a desired length of time (t_a). The films were then carbon-coated to improve their stability under the electron beam.

To minimize radiation damage of organic crystals, a Jeol JEM 2000-EX transmission electron microscope, equipped with a high-resolution polepiece and LaB_6 filament, was operated at 200 keV. The diameters of the condenser and objective apertures were set at 300 and 20 ± 5 μm, respectively, and selected-area electron diffractograms (SAEDs) were obtained using a nominal camera length of 120 cm and a 300 μm field-limiting aperture. Dark-field imaging conditions that permitted successful recording of crystallites were limited primarily by the radiation sensitivity of the crystallites themselves [19]. Consequently, the optimal magnification range for observing (focusing) and recording the crystallites in the HMW copolymer was kept between 8000× and 10000×, but this was reduced to 6000 to 8000× for the LMW material. Most micrographs presented here were acquired by using low dosages and "shooting blind" (i.e. focusing on one area and then recording an adjacent, undamaged region). Information on the radiation sensitivity of the crystallites was obtained by recording the current beam density of a bright-field image on the small viewing screen in the microscope and the time of exposure to the electron beam. Assuming an ideal electron collection efficiency at the screen, the resultant electron density in the sample plane was determined by the general method described in the literature [20–22].

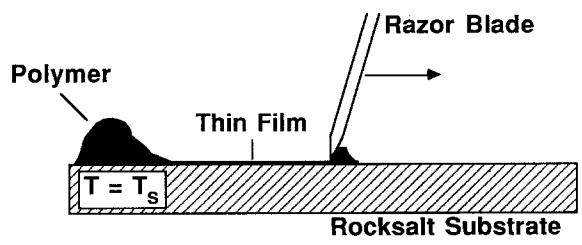

Figure 2 Illustration of the technique used for preparing ultrathin films of B–N copolymers suitable for conventional TEM study. The temperature at which the shearing is performed is denoted T_s.

Microdensitometry was performed using a Joyce-Loebl digital scanning microdensitometer (Technical Operations, Inc., Burlington, Massachusetts, USA) set on a 100 μm spot size. Measurements and contour mapping of the resulting images, which typically occupied frames of 512 × 512 pixels, were performed using the Semper VI image analysis algorithm by Synoptics Ltd.

3. Results

3.1. Imaging of crystallites from the HMW copolymer

All of the micrographs in this section were obtained from samples sheared in the fluid mesophase, with $T_s = 310°$ C, and subsequently annealed for a short time ($t_a = 30$ min) at a temperature above the T_g in the solid state ($T_a = 200°$ C). A typical SAED pattern obtained from a region about 2.5 μm in diameter from the HMW B–N copolymer is presented in Fig. 3. It is clearly evident that the average molecular orientation is well aligned in the direction of the shear (vertical). The third meridional reflection is more laterally diffuse than the first, suggesting some degree of imperfection in the longitudinal register between the chains in the crystallites [11]. Measurement of the meridional reflection spacings shows that the position of the third peak is not a simple multiple of the first, with the ratio of scattering vectors between the first and third along the meridian being approximately 0.32. The significance of this fact is that the intrachain spacing is aperiodic, i.e. the copolymer is indeed random, in agreement with other reports on this material [1–5, 9, 11].

Fig. 4 is a series of electron micrographs taken from different regions of the specimen on account of radiation damage and imaged using selected areas of the back focal plane, as illustrated in Fig. 4a. Fig. 4b is thus the bright-field (BF) image, and Figs 4c to f demonstrate dark-field (DF) microscopy: the equatorial reflection (labelled c in Fig. 4a), the "wing" off-axis region (d), the intrachain meridional region (e) and the third meridional reflection (f). DF imaging utilizing the first meridional spot was severely hindered by the proximity of the reflection to the centre beam spot and by its relatively rapid fading during irradiation.

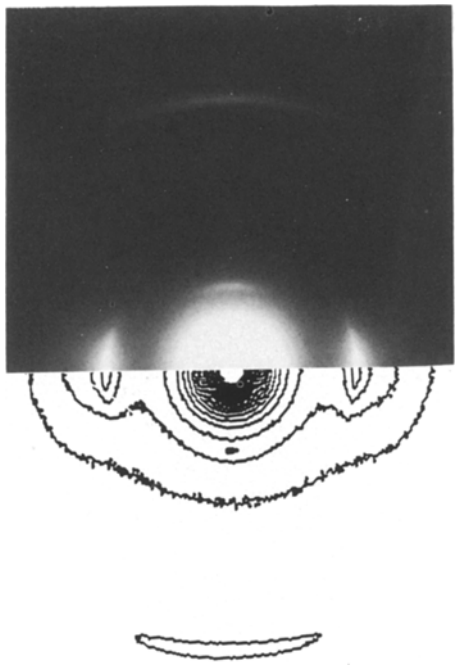

Figure 3 Selected-area electron diffractogram (SAED) of the HMW B–N copolymer demonstrating the orientation of the molecular axis (vertical), the randomness of the molecular chains (aperiodic meridional maxima), and the finite degree of lateral ordering (equatorial reflections).

To maintain the same level of radiation damage and thereby facilitate comparison between the micrographs in Fig. 4, the regions recorded were all free from previous radiation damage and were exposed to similar radiation doses over the course of being recorded. An example of a BF image of the HMW B–N copolymer is presented in Fig. 4b. Contrast variations in this mode of imaging are principally due to variations in atomic composition or specimen thickness. Since the composition of this copolymer is expected to be uniform, thickness variations are likely to be responsible for contrast observed in BF micrographs, with the darker regions representing thicker areas of the specimen. These variations are quite useful in determining the direction of shear, which will be kept vertical in all of the micrographs presented in this work.

The DF image shown in Fig. 4c was acquired by tilting the beam so that the central region of the equatorial reflection was centred in the objective aperture. Bright features, measuring approximately 20 nm thick and 60 nm long, appear to be oriented with their short axes parallel to the shear direction, which is confirmed to be the molecular chain axis [23] by the diffraction patterns. Since the bright features are seen only in DF images, they would appear to be the diffracting entities producing the sharp diffraction maxima, such as the equatorial reflection, in the SAED pattern and therefore demonstrate the presence of crystalline order. Since these entities are discrete and spaced at irregular intervals, it is reasonable to conclude that they may very well be NPL crystallites. Indeed, their disposition is strikingly similar to the modelling predictions of Hanna and Windle [10].

Fig. 4d shows the results of imaging in the off-axis "wing" region of the equatorial reflection. Orientation contrast is paramount, and a banded texture [13, 14, 17] is revealed with a periodicity, measured along the shear direction, of about 0.24 μm. When the beam is tilted to the region between the meridional maxima (e in Fig. 4a), the resulting DF image (Fig. 4e) also displays diffracting structure oriented normal to the shear direction. Although not nearly as pronounced or regular as the bands, part of this observed pattern is on the same size scale as that of the bands, while there is a distribution of diffuse spots in the background (which are not as sharply defined as the crystallites in Fig. 4c). Upon tilting the beam further along the meridian so that the centre of the third meridional arc is centred in the objective aperture, very little contrast is seen in the DF image (Fig. 4f). Dark patches do suggest the presence of areas that are not contributing to this diffraction arc.

It must be pointed out that Figs 4d to f have had their contrast enhanced to facilitate viewing of low-contrast structure. Intensity measurements of structural features in the corresponding digitized micrographs reveal that the crystallites in Fig. 4c are approximately 21% more intense than the background, whereas the diffracting structures in Figs 4d and e exceed the background level by about 12 to 13%. Contrast variations in Fig. 4f do not differ by more than 3%.

The failure to image the entities in the much weaker meridional reflections, or even in BF, is considered to be an experimental problem associated with the resulting beam damage of the polymers and should not be interpreted in terms of a lack of correlation between the laterally sharp meridional reflections and diffracting entities. Indeed, recent studies [24] of a closely related but more beam-resistant polymer have demonstrated the presence of crystallites in both DF, in the meridional reflections as well as in the equatorials, and in BF. The fact is clear that the small entities are only imaged in strong, sharp features of the diffraction pattern. This point, coupled with the observation that the diffraction maxima fade at much the same rate upon irradiation, strongly indicates that they represent crystals.

3.2. Crystallite characteristics

Since these NPL crystallites are observed only when the equatorial reflection is used for DF imaging, the remaining micrographs in this work will be DF images utilizing this particular reflection. Thickness variations in the sample can, however, be detrimental to the clarity of the crystallites, with thicker regions superimposing many potential images. Fig. 5 demonstrates the result of tilting the specimen 20° along a single-tilt axis within the microscope. In this case, the tilt axis is estimated to be about 53° from the shear direction. The crystallites, still oriented normal to the shear direction, appear thicker than those seen earlier and measure about 30 nm thick and 60 nm long. The variation in crystallite shapes between Figs 4c and 5 (which were both from the same specimen) is indicative of the crystallites being plate-like, since tilted projections would simply expose more of the crystallite

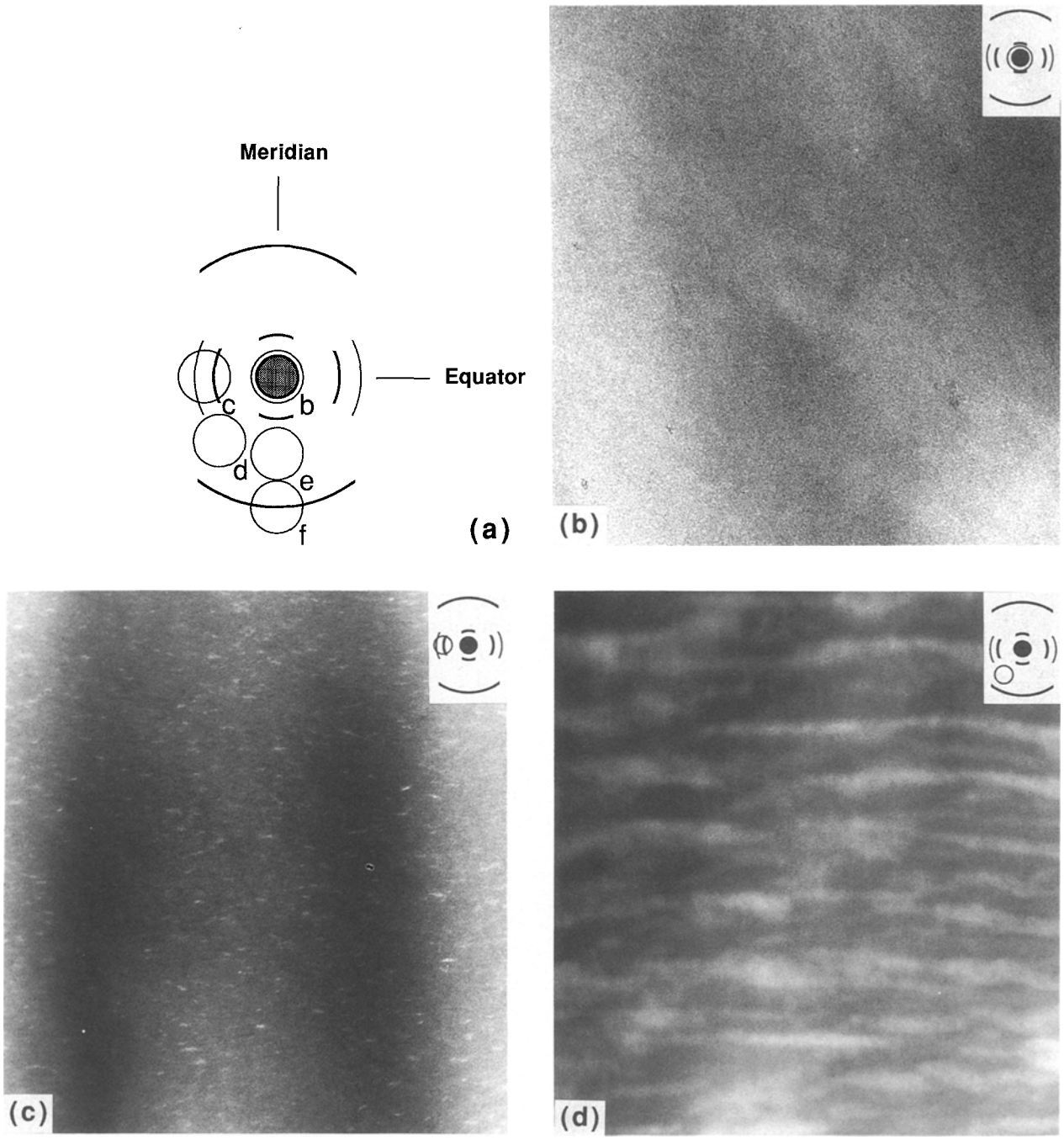

Figure 4 (a) Schematic diagram of the SAED typically exhibited by the B–N copolymer showing the locations of the objective aperture in DF imaging (as described in the text). (b) A BF electron micrograph, using the central beam spot in (a). The remaining micrographs were acquired by DF imaging in (c) the equatorial reflection, (d) the off-axis "wing", (e) the intrachain region and (f) the third meridional arc. The small SAED schematic diagram on each micrograph designates which region is responsible for the DF image. Contrast enhancement of Figs 4d to f, necessary to facilitate the viewing of low-contrast structure, is discussed in the text.

surface to the electron beam, as is seen in Fig. 5. As in Figs 4d to f, the contrast has been slightly enhanced in this micrograph (Fig. 5) due to the loss of contrast attributable to the increased sample thickness in the direction of the electron beam. Here, the average crystallite intensity exceeds the background intensity by about 19%.

The relationship between these crystallites and the banded texture is seen in Fig. 6. It is of interest to note that the crystallites, lying normal to the local molecular director, appear to be absent from banded areas which are almost completely non-diffracting (dark). These dark regions are areas where the structure is misoriented and would diffract into the wings of the equatorial diffraction peak, which are not included in the aperture. The absence of crystallites in these regions would imply that they are misoriented in concert with the matrix.

3.3. Effect of thermal history

In this section, the effect of varying these factors is examined. The micrographs presented in Fig. 7 have all been obtained from samples keeping $T_s = 310°$ C. In Fig. 7a, the image reveals the results of shearing and immediately quenching a specimen without any subsequent annealing. The presence of crystallites, although not as well-formed as those previously seen, is in accord with differential scanning calorimetry,

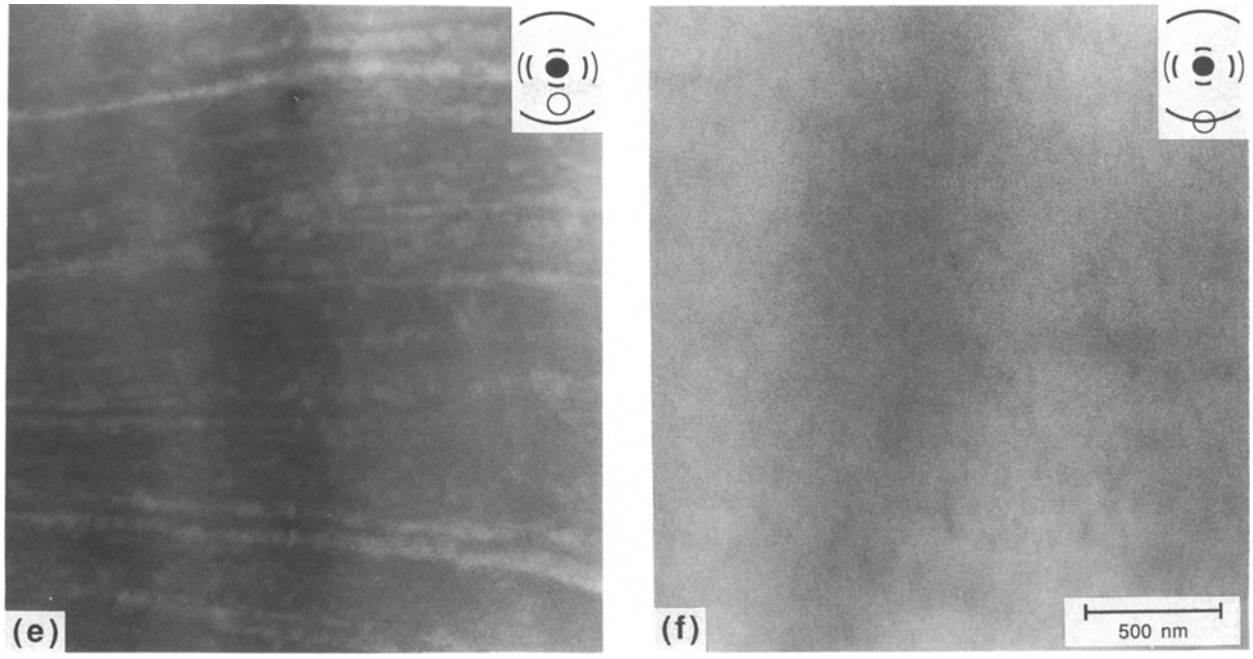

Figure 4 Continued.

which suggests that quenching is unable to suppress crystallization in these materials.

Annealing specimens such as the one shown in Fig. 7a for 30 min at $T_a = 200°$ C results in the crystallite structure observed in the previous micrographs and is presented in Fig. 7b for the sake of comparison. Long-term annealing ($t_a = 480$ min) at the same T_a, as is seen from Fig. 7c, appears to increase the number density of crystallites (i.e. the number of crystallites per unit area observed), and there is some indication that the crystals are slightly thicker. It should also be noted that there is no evidence of large-scale crystal growth. However, as is expected [1], the degree of crystallinity in the long-annealed sample presented in Fig. 7c is estimated to be significantly higher than that in the short-annealed one in Fig. 7b; but the increase is not as dramatic as the crystallite formation during the short-term anneal, indicating that most of the primary crystallization occurs during short time spans of annealing above T_g. Annealing a specimen at a higher temperature ($T_a = 250°$ C) for 60 min yields the crystallites observed in Fig. 7d. The primary differences between the crystallites acquired by annealing at 200° C and those obtained at $T_a = 250°$ C, with the latter averaging about 20 nm thick and 80 nm long, are the clarity and increased length of those annealed at the higher temperature. When T_a is increased even further

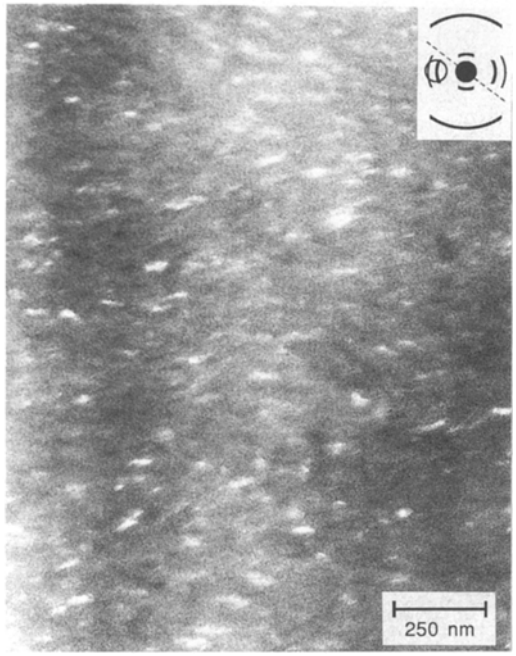

Figure 5 DF image of a sample that has been tilted 20° along a single-tilt axis within the electron microscope. The tilt axis is shown in the SAED insert.

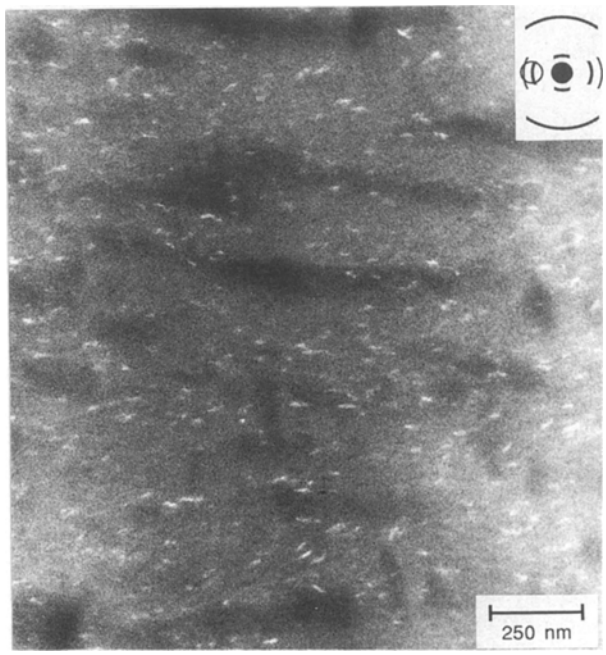

Figure 6 DF micrograph demonstrating the relationship between the supramolecular "banded" texture and NPL crystallites. The dark bands correspond to regions of maximum misorientation about the shear axis. It is significant that few crystallites are imaged in these regions, confirming that there is close correlation between the molecular chain axes in the crystals and the matrix.

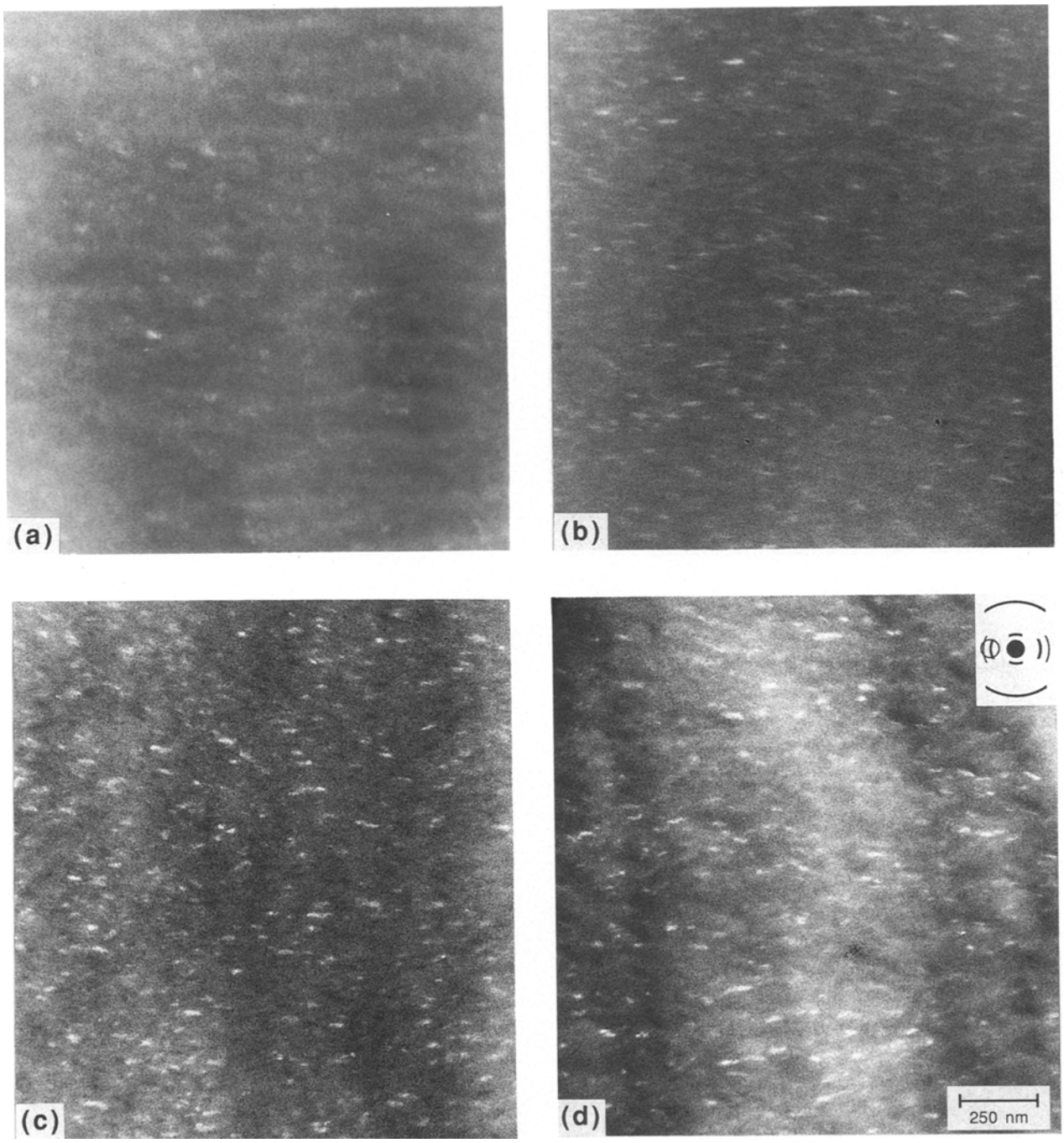

Figure 7 DF images of an annealing sequence of HMW samples sheared at 310° C. (a) The sample received no subsequent annealing. (b) Annealing for 30 min at 200° C results in a significant increase in crystallites. (c) Extended annealing for 480 min produces a continued, but more moderate, increase in the crystallite population. (d) Increasing T_a to 250° C and keeping t_a = 30 min yields crystallites which appear somewhat thinner and longer than those in (b).

still to 300° C (which is above T_m), the ultrathin films can no longer maintain sufficient structural integrity and collapse into fibrils that are not electron-transparent.

The micrographs seen in Fig. 8 are obtained from samples where T_s has been increased to 350° C (approximately 60 to 70° C above their T_m). A small volume fraction of comparatively long crystallites is apparent in the samples which were unannealed, as shown in Fig. 8a. Increasing the annealing time to 30 min at 200° C (Fig. 8b) and 250° C (Fig. 8c) results, once again, in a large increase in the crystallite population. As in the previous case (when T_s = 310° C), long-term annealing does not significantly alter the crystallite morphology but does increase the degree of crystallinity.

3.4. Effect of molecular weight

A typical SAED of the LMW B–N copolymer is presented in Fig. 9. As has been reported elsewhere [5], the positions of the principal meridional and equatorial reflections are the same as those observed in the HMW analogue; however, the material is not as well oriented. Off-axis reflections have been observed in diffraction patterns of this material, suggesting three-dimensional crystallinity; this issue, however, is to be discussed elsewhere [25].

DF imaging in the centre of the equatorial reflection once again results in the appearance of diffracting entities, as seen in Fig. 10. The crystallites in Fig. 10a differ considerably from those exhibited by the HMW copolymer, by appearing a little thinner but considerably

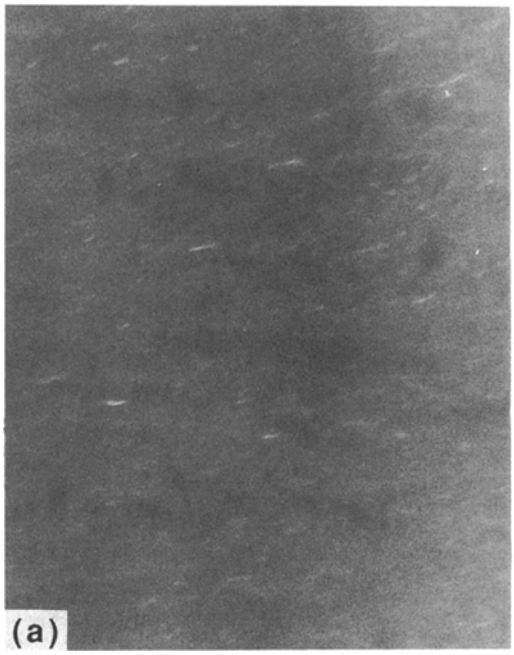

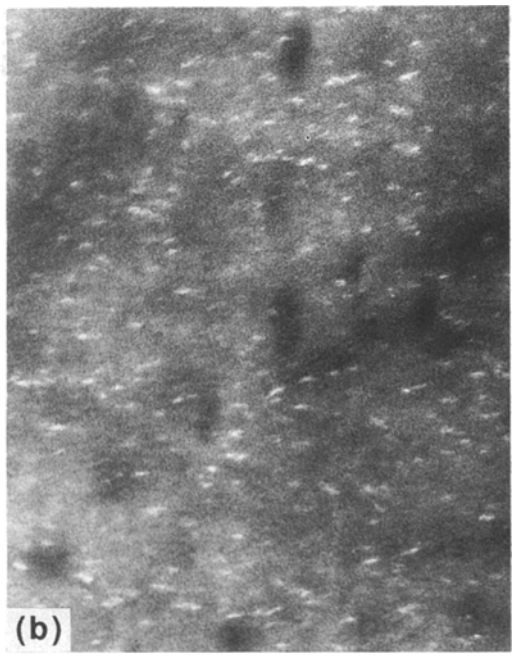

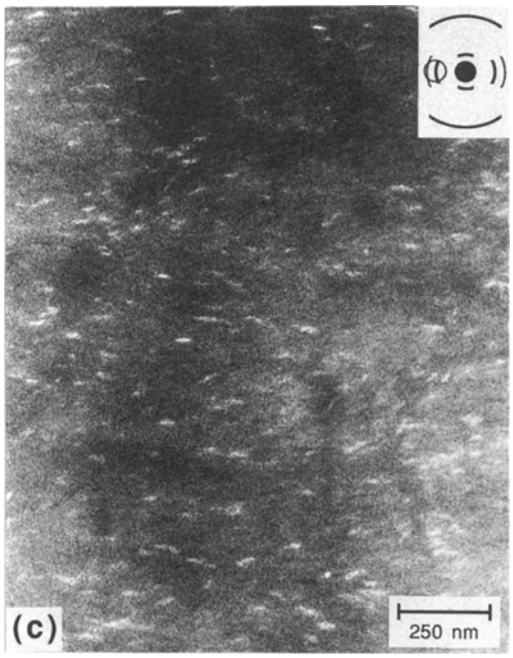

Figure 8 Annealing sequence of DF micrographs when T_s is increased to 350° C. (a) Crystallites persist even when $t_a = 0$ min. Subsequent annealing for 30 min at (b) 200 and (c) 250° C results in a significant crystallite population.

longer, averaging approximately 10 nm thick and 200 to 300 nm long. The length of these crystallites is almost 3 to 5 times the length of those seen earlier in this work for the HMW copolymer. Their thickness is of the order of the molecular length ($\approx$ 16.5 nm) but varies more or less at random along the crystallite length. The "dark" discrete features which appear in Fig. 10 are presumed to be crystallites diffracting outside the aperture and are discussed later.

It should be noted that Fig. 10a and an enlargement presented in Fig. 10b (which clearly shows the jagged edges of the crystallites) represent the copolymer sheared well below its T_m ($\approx$280 to 290° C) at T_s = 200° C and subsequently annealed for 30 min at the same temperature. Under these conditions, which are identical to those used by Donald and Windle [12] to obtain crystallite images in an HMW 70 : 30 B–N copolymer, the act of shearing is actually conducted against a solid, rather than against a fluid. Shearing above T_s, followed by annealing at $T_a < T_m$, results in crystallites more structurally similar to those seen in the HMW material but still remaining significantly longer [25].

4. Discussion

According to Sawyer and Grubb [22], the three most important classes of liquid-crystalline polymers include the aromatic polyamides, the "rigid rod" polymers, and the aromatic copolyesters. The first two categories refer to lyotropic polymers, which require the presence of a solvent to exhibit liquid-crystalline flow characteristics; the last refers to a class of liquid-crystalline polymers that can be thermally processed in a mesophase melt. Studies of poly(phenylene terephthalamide) (PPTA) [26], the Kevlar aromatic polyamide, and of poly(*p*-phenylene benzobisthiazole) (PPBT) [27], an example of a "rigid rod" polymer, have revealed the presence of crystallites, oriented along the molecular axis, in these materials. Recently, investigations of Mazelet and Kléman [28] have shown that crystallites also form but appear normal to the molecular axis in a thermotropic homopolyester exhibiting a nematic phase. However, the crystallites first imaged by Donald and Windle [12] and now characterized here are unique in that they form in a *random* thermotropic aromatic copolyester.

Despite variations due to the processing conditions mentioned earlier, the average crystallite size in the HMW B–N copolymer is approximately 20 nm thick (in the chain direction) and 60 nm long, in agreement with the previous report [12]. It should be emphasized, however, that the crystallites reported here for the HMW material are obtained when samples of the copolymer were (i) sheared above its T_m and (ii) annealed in the absence of any substrate. The presence

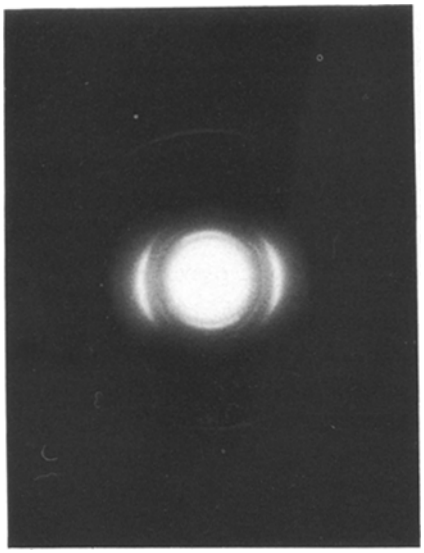

Figure 9 SAED of the LMW B–N copolymer, exhibiting reflections similarly spaced [5] as in Fig. 3. The arcing of the equatorial reflection in particular is indicative of a broad distribution of lateral periodicities.

of a substrate has dramatic effects on microstructural growth in ultrathin polymeric films, especially if the specimen thickness is of the same magnitude as the chain length. The most important of these effects in B–N films undergoing annealing is homeotropy, in which a polymer chain tends to orient normal to the substrate surface [15]. The presence of the KCl substrate during annealing may explain why crystallites were not noticed [12] in specimens that had been sheared at 300° C or higher. In addition, the domains, boundaries and veins reported [15–17] for B–N copolymers annealed on KCl are not observed in the films of the HMW copolymer produced here. Problems associated with the absence of any supportive substrate, such as film retraction [17], have not been encountered in this study during annealing at temperatures more than 50° C below the T_m of the copolymer, although some evidence of twisting [16] may be evident in the LMW material [25].

The most significant hindrance in obtaining electron micrographs representative of the crystallite morphology and population has been the radiation sensitivity of the copolymer to the electron beam. While a detailed study of this effect will be presented elsewhere, it is worth noting the dose levels used in this work, as estimated from knowledge of the current beam density at the image plane and the calibrated magnification [21, 22]. Assuming an ideal screen collection efficiency, the doses of the BF image (Fig. 4b) and DF images (Figs 4c to f) are of the order of $660 \pm 200\,\mathrm{Cm}^{-2}$.

Radiation damage in organic crystals is responsible for crystalline diffraction spots fading and/or broadening with dose and is, consequently, more apparent in DF imaging than in BF [19]. According to Grubb [20], intramolecular spacings tend to persist longer than crystalline order during irradiation. The observed rapid broadening of the principal equatorial reflection is consistent with this trend. The first meridional reflection becomes engulfed in an enlarging central halo, while the third meridional arc remains the longest and eventually spreads to a full halo. In the case of the HMW copolymer, the crystallites are noted to always fade before the conclusion of the recording step; thus, there is an inherent degree of distortion in the micrographs, even though operating at 200 keV reduces the radiation damage in organic specimens by about 37% compared with 100 keV [21]. A reduction

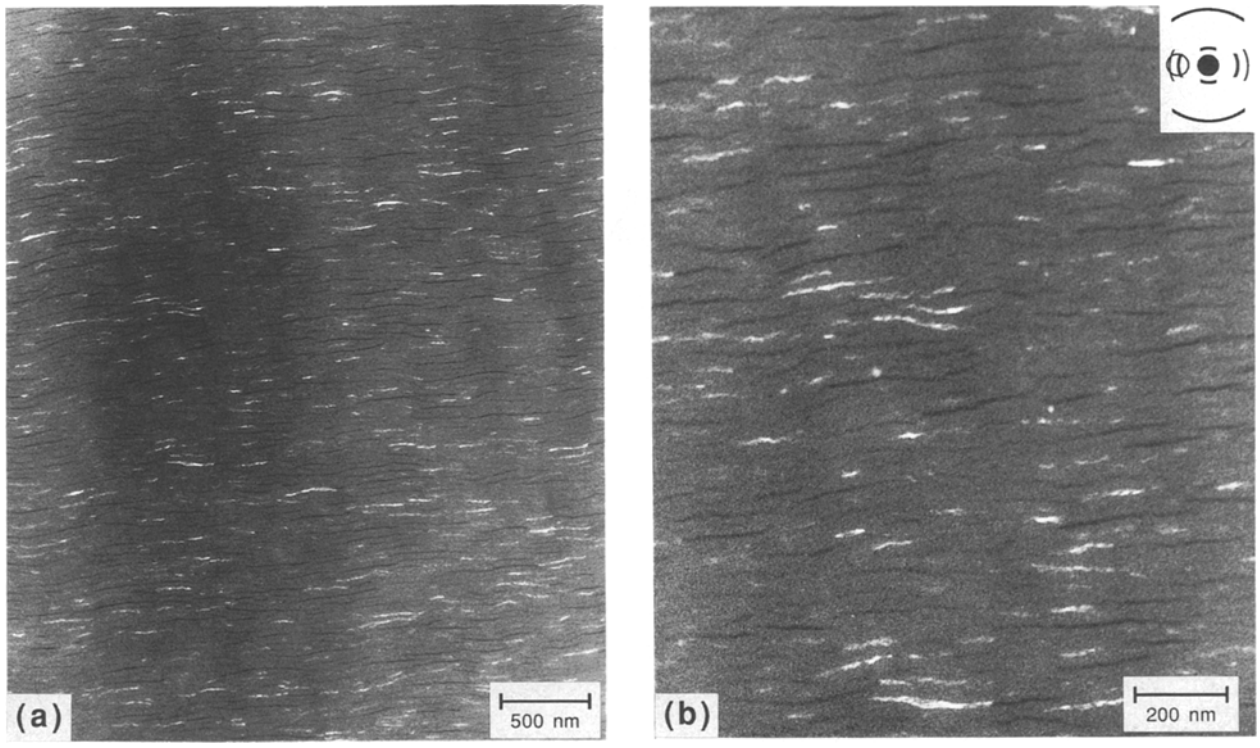

Figure 10 DF micrographs of the LMW B–N copolymer as imaged in the equatorial reflection. (a) Crystallite orientation in a sample which was both sheared and annealed at 200° C (approximately 80° C below its T_m). (b) Morphology of individual crystallites in an enlargement of (a).

in the magnification necessary to observe crystallites in the LMW material has allowed the use of lower doses, resulting in the retention of some crystallite structure beyond a single exposure.

The observation that the fading of the diffracting entities is correlated with the broadening of the equatorial halo supports the conclusion that it is organic crystals that are being imaged, albeit imperfect ones. The annealing sequence (Fig. 7) of the HMW copolymer sheared at 310° C and annealed at 200° C provides insight into crystallite formation. Even without subsequent annealing, the sheared sample in Fig. 7a exhibits some crystalline order, which is the result of either (i) crystallite preservation beyond T_m, (ii) crystallite formation during the shearing action, or (iii) crystallite formation during the rapid quench. Although it has been demonstrated [9] that crystalline order in these copolymers can be increased by shearing, evidence also exists [6] that some crystallization occurs even in samples that have been quickly quenched. Annealing a sheared specimen for even a short period of time at 200° C (Fig. 7b) results in a drastic increase in crystallites. Long-term annealing is seen to produce more crystallites but does not seem to alter significantly the crystallite morphology, as is evident from Fig. 7c. Thus, it can be reasonably concluded that the crystallites undergo significant development during the early stages of annealing, suggesting that the formation of these physical crosslinks hinders the translational motion of adjacent chains necessary for further lateral sequencing. This observation supports the nucleation model proposed by Blundell [6], in which the initial formation of crystallites hinders chain diffusion, thereby retarding crystallite growth and crystalline perfection. Crystallization in these copolymers has also been explained [8] in terms of a two-step process, the first of which is fast and occurs on the order of seconds and the second of which is very slow (of the order of 10^7 sec).

Attempts at discerning the crystallization in B–N copolymers from X-ray analysis have resulted in estimates of 21% in a 40 : 60 copolymer [6] to 30 to 60% (depending on annealing conditions) for a 58 : 42 sample [8]. However, it is difficult to quantify the crystallinity of the HMW copolymer in this study from electron micrographs; suffice it to say that it is probably as high as 15% and certainly much less than 50%.

It is apparent from Fig. 10 that the crystallinity is higher in the LMW copolymer than in the HMW analogue. According to the predictions made by Hanna and Windle [10], the crystallinity is expected to increase as the DP decreases, due to facilitated lateral alignment of the shorter chains. Since the NPL crystallites in Fig. 10 seem to be located in one of the thinnest regions of the ultrathin film, it is reasonable to estimate a crystallite separation distance. Before doing so, though, the nature of the "dark" entities observed in that micrograph must first be discerned.

One possibility is that the dark entities observed here, also seen in a closely related material [24], may indicate the presence of microtears. However, microtears normally lie in the direction of shear and exhibit fibrillar detail and are visible in BF imaging. The dark entities in Fig. 10 lie normal to the shear direction and are not observed in BF.

The remaining possibility with regard to the nature of these entities, which tend to appear in samples either sheared below T_m or sheared above T_m and annealed for long periods of time, is that they are crystallites diffracting outside the objective aperture. This may occur when some of the comparatively long equatorial arc due to crystallites lies outside the objective aperture. Another conceivable explanation for the absence of diffraction inside the aperture is that the molecules in the non-diffracting crystallites have some preferred orientation along the axis of the electron beam, similar to some of the supramolecular structures reported elsewhere [16, 17]. In either case, the dark entities dispersed between the diffracting crystallites are also believed to be crystallites diffracting outside the microscope aperture. Including them in the crystallite population of Fig. 10 yields an average separation distance of 75 nm, with a corresponding crystallinity of approximately 13%, assuming a film thickness equal to that of the crystallites (10 nm). It should be borne in mind that this value could still be an underestimate, since some crystallites may have been lost through damage during irradiation, even at the lower magnification employed. Hence, this value of the crystallinity is not thought to be inconsistent with an earlier value of 21% [6] or model predictions in the region of 20% [10].

5. Conclusions

The aim of this work has been to characterize the crystallites that develop in two thermotropic random copolymers with the same composition but different molecular weights. Crystallites in the HMW material are observed clearly only when the centre of the equatorial reflection is used for the DF imaging. Failure to image the crystalline entities in BF or in DF using the weak meridional maxima as sources of diffraction contrast is attributed to the beam sensitivity of the polymers. Unlike crystallites found in other liquid crystalline polymers [26, 27], the randomly distributed crystallites observed here, typically measuring 20 nm thick and 60 nm long, are oriented normal to the shear direction, i.e. the molecular chain axis. The fact that they are identified with aperiodic meridional maxima indicates that they are the non-periodic layer crystallites referred to in the literature [5, 9–12].

It has been found that shearing up to 60 to 70° C above the T_m of the copolymer (in the fluid mesophase), followed by a rapid quench to 0° C, does not preclude the existence of these crystallites, although subsequent short-term annealing (t_a = 30 min) above T_g in the solid state results in a noticeable increase in their number. Extended annealing (t_a = 480 min) yields a further increase in the crystallite population and in overall crystallinity, but the changes are less pronounced in terms of the crystallite morphology. Annealing at temperatures close to the melting point is seen to produce crystallites which appear thinner and longer than those found after lower-temperature treatments.

The LMW analogue exhibits a higher crystallinity than the HMW material, with crystallites typically measuring 10 nm thick and 200 to 300 nm long. Shearing below and above T_m produces crystallites that vary considerably in both structural detail and population. An estimate of the crystallinity in the LMW copolymer sheared and annealed below T_m, based on an apparent crystallite separation distance of 75 nm, is 13%, which is consistent with the predictions of Hanna and Windle [10].

Acknowledgements

The authors would like to thank the Hoechst-Celanese Corporation for supplying the materials and providing one of us (R.J.S.) with funding as an academic visitor. Sincere gratitude is expressed to Professor A. Howie and the Microstructural Physics Group (Cavendish Laboratory) for the use of the electron microscope and to Dr W. Stobbs for helpful discussions.

References

1. J. BLACKWELL, A. BISWAS and R. C. BONART, *Macromolecules* **18** (1985) 2126.
2. R. A. CHIVERS, J. BLACKWELL and G. A. GUTIERREZ, *Polymer* **25** (1984) 435.
3. J. BLACKWELL and G. GUTIERREZ, *ibid.* **23** (1982) 671.
4. G. R. MITCHELL and A. H. WINDLE, *Coll. Polym. Sci.* **263** (1985) 230.
5. T. J. LEMMON, S. HANNA and A. H. WINDLE, *Polym. Commun.* **30** (1989) 2.
6. D. J. BLUNDELL, *Polymer* **23** (1982) 359.
7. G. A. GUTIERREZ *et al.*, *ibid.* **24** (1983) 937.
8. G. D. BUTZBACH, J. H. WENDORFF and H. J. ZIMMERMANN, *ibid.* **27** (1986) 1337.
9. A. H. WINDLE *et al.*, *Faraday Disc. Chem. Soc.* **79** (1985) 55.
10. S. HANNA and A. H. WINDLE, *Polymer* **29** (1988) 207.
11. R. GOLOMBOK, S. HANNA and A. H. WINDLE, *Mol. Cryst. Liq. Cryst.* **155** (1988) 281.
12. A. M. DONALD and A. H. WINDLE, *J. Mater. Sci. Lett.* **4** (1985) 58.
13. A. M. DONALD, C. VINEY and A. H. WINDLE, *Polymer* **24** (1983) 155.
14. A. M. DONALD and A. H. WINDLE, *J. Mater. Sci.* **18** (1983) 1143.
15. A. M. DONALD, *J. Mater. Sci. Lett.* **3** (1984) 44.
16. A. M. DONALD and A. H. WINDLE, *Polymer* **25** (1984) 1235.
17. *Idem, J. Mater. Sci.* **19** (1984) 2085.
18. C. VINEY and A. H. WINDLE, *ibid,* **17** (1982) 2661.
19. E. L. THOMAS, in "Structure of Crystalline Polymers", edited by I. H. Hall (Elsevier Applied Science, London, 1984) Ch. 3.
20. D. T. GRUBB, *J. Mater. Sci.* **9** (1974) 1715.
21. L. REIMER, in "Physical Aspects of Electron Microscopy and Microbeam Analysis" edited by B. M. Siegel and D. R. Beaman (Wiley, New York, 1975) Ch. 13.
22. L. C. SAWYER and D. T. GRUBB, "Polymer Microscopy" (Chapman and Hall, London, 1987) pp. 62–70, 239–254.
23. C. VINEY, A. M. DONALD and A. H. WINDLE, *Polymer* **26** (1985) 870.
24. R. J. SPONTAK and A. H. WINDLE, *ibid.* (in press).
25. R. J. SPONTAK, T. J. LEMMON and A. H. WINDLE, manuscript in preparation.
26. M. G. DOBB, D. J. JOHNSON and B. P. SAVILLE, *J. Polym. Sci, Polym. Symp.* **58** (1977) 237.
27. J. R. MINTER, K. SHIMAMURA and E. L. THOMAS, *J. Mater. Sci.* **16** (1981) 3303.
28. G. MAZELET and M.KLÉMAN, *ibid.* **23** (1988) 3055.

Received 11 May
and accepted 12 September 1989